21st Australasian Fluid Mechanics Conference
Adelaide, Australia
10-13 December 2018

Aerosol Particle Transport and Deposition in a CT-Based Lung Airway for Helium-Oxygen Mixture

M. S. Islam[1], S. C. Saha[1] and P. M. Young[2]

[1]School of Mechanical and Mechatronics Engineering
University of Technology Sydney, Sydney, NSW-2007, Australia
[2]Respiratory Technology, Woolcock Institute of Medical Research and Discipline of Pharmacology, Sydney Medical School, The University of Sydney, 431 Glebe Point Road, Glebe, NSW 2037, Australia

Abstract

A precise understanding of the aerosol particle transport and deposition (TD) in the human lung is important to improve the efficiency of the targeted drug delivery, as the current drug delivery device can deliver only a small amount of the drug to the terminal airways. A wide range of available computational and experimental model has improved the understanding of particle TD in the human lung for air breathing. However, the helium-oxygen gas mixture breathing is less dense than the air breathing and the turbulent dispersion is less likely to develop at the upper airways, which eventually reduce the higher deposition at the upper airways. This study aims to investigate the effects of the helium-oxygen gas mixture at the upper airways of a realistic human lung. A realistic lung model is developed from the CT-Scan data for a healthy adult. A Low Reynolds Number (LRN) k-ω model is used to calculate the fluid motion and Lagrangian particle tracking scheme is used for particle transport. ANSYS Fluent solver (19.0) is used for the numerical simulation and MATLAB software is used for the advanced post-processing. The numerical results show that helium-oxygen gas mixture breathing reduces the aerosol deposition at the upper airways than the air breathing. The present simulation along with more case-specific investigation will improve the understanding of the particle TD for the helium-oxygen mixture.

Themes: Computational fluid dynamics, Multiphase and particle-laden flows, Turbulence, Biomedical fluid mechanics, Micro/biofluid mechanics.

Introduction

Heliox is the compound mixture of helium (He) and oxygen (O2) gas. Helium-oxygen (He-O2) gas mixture generates relatively less airway obstruction than the air and which eventually help to ventilate the lung airways with less mechanical energy [1]. The helium-oxygen mixture density (0.5 g/l) is noticeably lower than the air density (1.25 g/l) and the lower density of the heliox produce less turbulence at the local airways. The heliox mixture help to reduce the turbulence effects at the local tracheobronchial airways and which generates less resistance. The overall procedure minimizes the aerosol deposition at the upper airways due to lower turbulence and which accelerate the particle to the lower airways [2]. A wide range of numerical [3-5] and experimental [6, 7] studies illustrate that fluid flow becomes locally turbulent at the extrathoracic region and strong turbulence fluctuation occurs higher deposition at the upper airways. There are a quite fewer number of studies that have been considered helium-oxygen gas mixture for particle TD in the extrathoracic and tracheobronchial and deeper airways. A CFD study on aerosol particle TD in an oral extrathoracic airway shows lower deposition for helium-oxygen gas mixture than the air [1]. The CFD study also illustrates that pressure loss at the oral airway is lower for the helium-oxygen mixture than the air. Recently, another study considered helium-oxygen mixture for aerosol particle TD in human lung and they used the imaging data to analyze the particle TD [8]. An experimental study aerosol particle TD for helium-oxygen gas shows less deposition at the upper airways than the air-breathing [9]. It is expected that the heliox breathing will decrease the deposition at the upper airways and will increase the deposition efficiency (DE) at the lower airways. However, it is experimentally difficult to measure the realistic aerosol deposition at the tracheobronchial airways. No CFD and experimental studies have been conducted for aerosol particle TD in the realistic tracheobronchial airways for heliox breathing. This study aims to conduct a CFD simulation for aerosol particle TD in a CT-based upper airway model during heliox breathing. The primary aim of the present study is to improve the understanding of the aerosol particle TD for heliox breathing.

Geometry Generation

A realistic anatomical model is generated from the CT-DiCom images of a 51 years healthy adult. The truncated anatomical model consists of first three generation from the trachea. Medical imaging software AMIRA and Geomagic are used to visualize the CT-images and surface rendering respectively. Volume rendering technique is used for the segmentation purpose and orthoslices are created with appropriate slice number. An isosurface is created for better visualization of the branching pattern. Volren is created for the visualization of the volume rendering data. The raw materials are removed by setting an appropriate threshold. The rough and missing surfaces of the 3-D model are reconstructed by Geomagic software. SolidWorks software is used to convert the final 3-D anatomical model. Figure 1 shows the visualization of the CT images and constructed 3D model of the tracheobronchial airways.

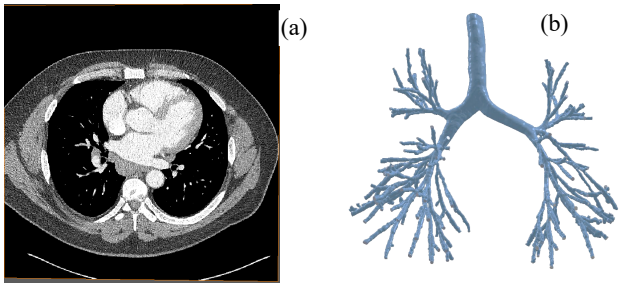

Figure 1: Realistic 3D anatomical model from CT-DiCom images; (a) CT-Scan data visualization and (b) 3D lung anatomical model.

Methods

The final airway model consists of three generations from the trachea. Ansys meshing module is used to construct the unstructured tetrahedral mesh for the highly complex asymmetric

model. A fine inflation layer mesh is employed near the wall for complex flow fields. An advanced meshing technique is used to generate the dense tetrahedral cells at the bifurcation area of the airway model. High smoothing techniques are used and the minimum size of the mesh is 1.002e-7m. A group of computational meshes is generated and tested for pressure variation. The final set of mesh contains about 3.44 million cells. Finite volume method is used for the numerical calculations and ANSYS 19 solver is used for the calculations. Euler-Lagrangian based Discrete Phase Model (DPM) and species transport model are considered to calculate the microparticle transport and deposition in the upper airways. The air is considered as the primary phase and the particle is the secondary phase in DPM. The equation for conservation of mass can be written as follows:

$$\frac{\partial \rho}{\partial t} + \nabla \cdot (\rho \vec{v}) = S_m \tag{1}$$

The source S_m is the mass added to the continuous phase from the dispersed second phase and any user-defined sources. The conservation of momentum in an inertial (non-accelerating) reference frame is described by;

$$\frac{\partial}{\partial t}(\rho \vec{v}) + \nabla \cdot (\rho \vec{v}\vec{v}) = -\nabla p + \nabla \cdot \left(\mu \left[\left(\nabla \vec{v} + \nabla \vec{v}^T \right) - \frac{2}{3} \nabla \cdot \vec{v} I \right] \right) + \rho \vec{g} + \vec{F} \tag{2}$$

where p is fluid static pressure, $\rho \vec{g}$ is body force due to gravity, and $\vec{F}$ is body force due to external (particle-fluid interaction) force. The stress tensor is associated with the molecular viscosity (μ) and the unit tensor (I).

The chosen k-ω model is based on the Wilcox [10], which incorporates modification of compressibility, low-Reynolds number effects and shear flow spreading. This is also based on model transport equations for turbulence kinetic energy (k) and the specific dissipation rate (ω).

Turbulence kinetic energy and specific dissipation rates are obtained from the following transport equations:

$$\frac{\partial}{\partial t}(\rho k) + \frac{\partial}{\partial x_i}(\rho k u_i) = \frac{\partial}{\partial x_j}(\Gamma_k \frac{\partial k}{\partial x_j}) + G_k - Y_k + S_k \tag{3}$$

and

$$\frac{\partial}{\partial t}(\rho \omega) + \frac{\partial}{\partial x_i}(\rho \omega u_i) = \frac{\partial}{\partial x_j}(\Gamma_\omega \frac{\partial \omega}{\partial x_j}) + G_\omega - Y_\omega + S_\omega \tag{4}$$

where G_k is the turbulence kinetic energy due to mean velocity gradients, G_ω is the generation of ω . Γ_k and Γ_ω are the effective diffusivity of k and ω, respectively. Y_k and Y_ω represent the dissipation of k and ω due to turbulence respectively. S_k and S_ω are source terms.

The effective diffusivities for the k-ω model are given by

$$\Gamma_k = \mu + \frac{\mu_t}{\sigma_k}$$
$$\Gamma_\omega = \mu + \frac{\mu_t}{\sigma_\omega} \tag{5}$$

where σ_k and σ_ω are turbulent Prandtl numbers, and μ_t is turbulent viscosity defined by

$$\mu_t = \alpha^* \frac{\rho k}{\omega} \tag{6}$$

Low Reynolds correction is used for the k-ω option. The coefficient α^*, damps turbulent viscosity, causing a low Reynolds number correction, which is given by

$$\alpha^* = \alpha_\infty^* \left(\frac{\alpha_0^* + \mathrm{Re}_t / R_k}{1 + \mathrm{Re}_t / R_k} \right) \tag{7}$$

The species transport equation for i[th] species

$$\frac{\partial}{\partial t}(\rho Y_i) + \nabla . (\rho \vec{v} Y_i) = -\nabla . \vec{J}_i + R_i + S_i \tag{8}$$

where the net rate of production of species i is R_i and S_i is the rate of creation by addition from the dispersed phase plus any user-defined sources. An equation of this form is solved for n-1 species where n is the total number of fluid phase chemical species present in the system. Since the mass fraction of the species must sum to unity, the n th mass fraction is determined as one minus the sum of the n-1 solved mass fractions. To minimize numerical error, the n^{th} species is selected as that species with the overall largest mass fraction.

The mass diffusion for the turbulent case is defined as;

$$\vec{J}_i = -(\rho D_{i,m} + \frac{\mu_t}{Sc_t}) \nabla Y_i - D_{T,i} \frac{\nabla T}{T} \tag{9}$$

where S_{Ct} is the turbulent Schmidt number.

The numerical investigation is performed for heavy physical activity condition (60lpm flow rate) and different diameter microparticles are considered. The particle density is used as $1100\ kg/m^3$. The overall calculations are carried out for air and helium-oxygen mixture. 80% helium and 20% oxygen is used for the mixture model. The velocity inlet and outflow outlet boundary condition are used in this study. The stationary wall and no-slip shear condition are used. The wall DPM boundary condition is used as trap and heat flux thermal condition is used at the wall.

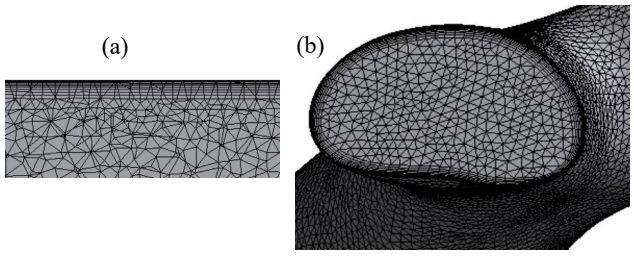

Figure 2.(a) Cross-sectional view of the inflation layer of the tracheal wall, and (b) outlet mesh at generation 3.

A comprehensive validation for microparticle TD is performed and the detail validation can be found in our previous study [11].

Results and Discussions

This study performed microparticles TD in an upper airway model for both air and helium-oxygen breathing. The overall numerical calculations are carried out for a higher flow rate. 1-µm and 10-µm diameter particles are considered for the present study.

The velocity profile for both air and heliox models are plotted at a selected line in the trachea. Figure 3 shows the velocity profile for air and heliox along z position. The calculated velocity profile for air and helium-oxygen breathing is different at the same position of the trachea however, the flow rate and anatomical model is the same for both cases. The overall velocity profile illustrates higher velocity magnitudes near the tracheal wall for

air-breathing than the helium-oxygen breathing. On contrary, velocity magnitude at the middle of the truncated tracheal airway is found higher for helium-oxygen breathing than the air breathing. For better illustration, velocity contours at the selected planes of the upper airway model are investigated for both cases. Figure 4 shows the velocity contours at different planes along with the flow vectors. The general velocity contour shows a similar velocity distribution at the selected planes. Plane 1 and plane 2 depicts the velocity magnitude near the wall for air-breathing is higher than the helium-oxygen breathing and which is also similar to the velocity profile in figure 3. The higher velocity magnitude near the wall for air-breathing influences higher deposition at the upper part of the tracheal wall.

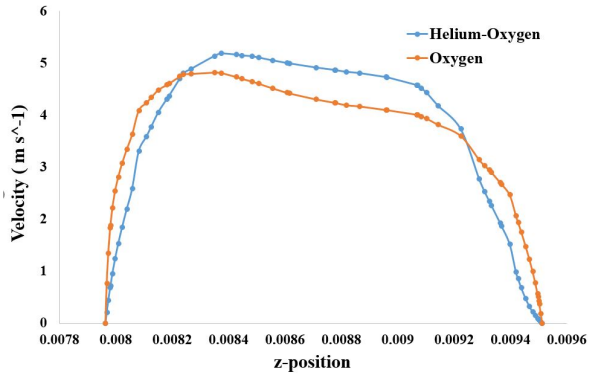

Figure 3: Velocity profile at the selected line of first bifurcation for air and heliox breathing.

Particle deposition pattern for 1-µm and 10-µm diameter particles are investigated, and figure 5 shows the microparticle deposition pattern for air and helium-oxygen breathing. Figures 5(a, b) show the deposition pattern for 10-µm diameter particle for air and helium-oxygen respectively. Figures 5 (c, d) show the deposition pattern for 1-µm diameter particles for air and helium-oxygen respectively. The overall deposition visualization shows a significant amount of microparticles are deposited at the tracheal wall compare to the right lung and left lung for both cases. For air-breathing, a significant amount of 10-µm particles are deposited at the very upper position of the trachea and less number of particles are deposited at the tracheal wall. On contrary, for helium-oxygen breathing, less number of particles are deposited at the upper part of the tracheal inlet and higher number of particles are deposited at the tracheal wall. The overall deposition pattern at the right lung and the left lung also shows higher deposition for air-breathing than the helium-oxygen breathing. A similar deposition pattern is observed for 1-µm diameter particles. The overall deposition at the tracheal wall, right lung and left lung show higher deposition for air-breathing than the helium-oxygen breathing. For 1-µm diameter particles, less number of particles are deposited the top of the trachea and higher number of particles are deposited at the tracheal wall. Microparticles inertia and inertial impaction play a critical role in the deposition at the upper airways. At 60 lpm flow rate, higher density of the air and microparticle inertia influence the deposition pattern. On contrary, the helium-oxygen gas mixture is less dense than the air and the lower density helps the particles not to deviate from its path line.

Figure 6 presents the DE for different diameter particles during air and helium-oxygen breathing. The total DE for 1-µm and 10-µm particles during different breathing is shown in figure 6(a). The general DE pattern shows higher deposition for air-breathing than the helium-oxygen breathing. The total DE comparison illustrates a significant amount of 10-µm diameter particles are deposited for air-breathing than the helium-oxygen breathing. The higher density of the air influences the overall deposition pattern for larger diameter particle. Figure 6(b) shows the DE comparison at the trachea, right lung and the left lung for different breathing. The DE comparison shows a significant amount of particles are deposited at the trachea compare to the right lung and the left lung. Microparticles inertia and higher density of the corresponding fluid density influence the overall deposition pattern at the highly complex tracheal wall. The DE chart also illustrates that higher percentage of particles are deposited at the right lung compare to the left lung. However, the right lung of the present model contains less branches than the left lung. The highly asymmetric structure of the realistic model, turbulent fluctuation and microparticle inertia influence the total deposition at the right lung. The DE chart (Figure 6(b)) depicts that higher percentage of particles are deposited at the right lung and the left lung for air-breathing than the helium-oxygen breathing irrespective to the particles diameter.

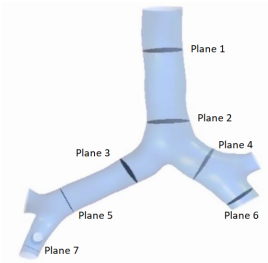

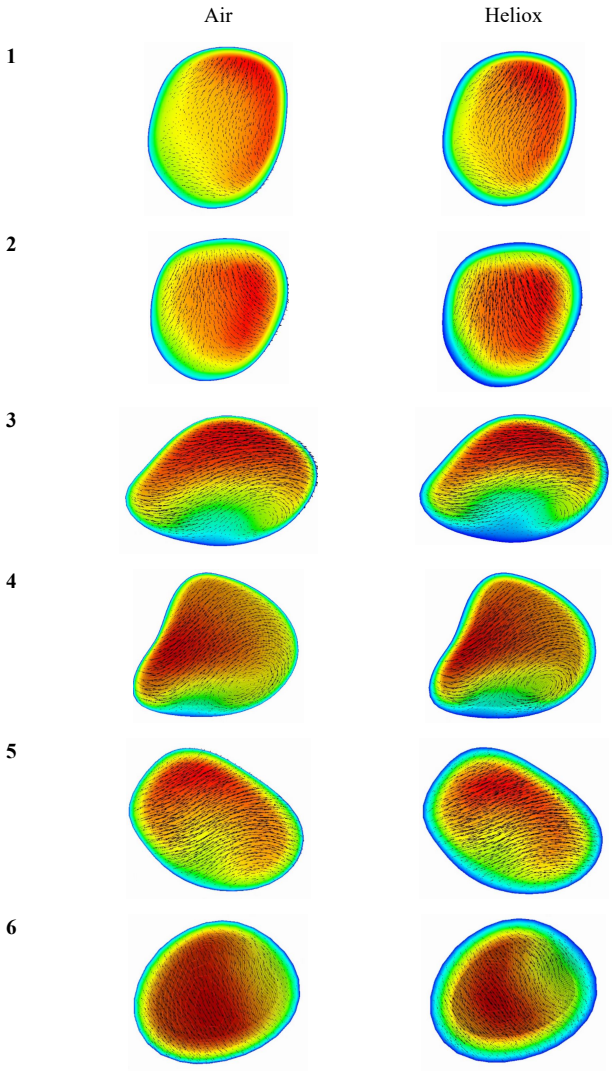

Figure 4: Velocity contour at different selected planes of the realistic geometry.

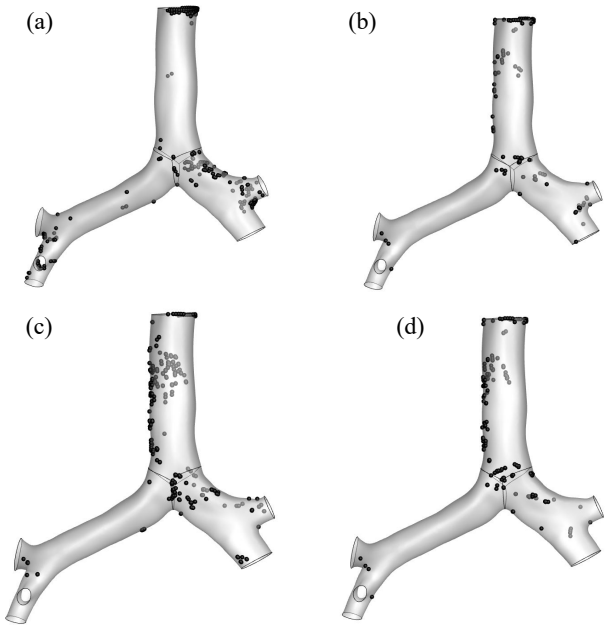

Figure 5: Microparticle deposition pattern for heliox and air-breathing at 60 lpm flow rate, (a) 10-µm air, (b) 10-µm heliox, (c) 1-µm air, and (d) 1-µm heliox.

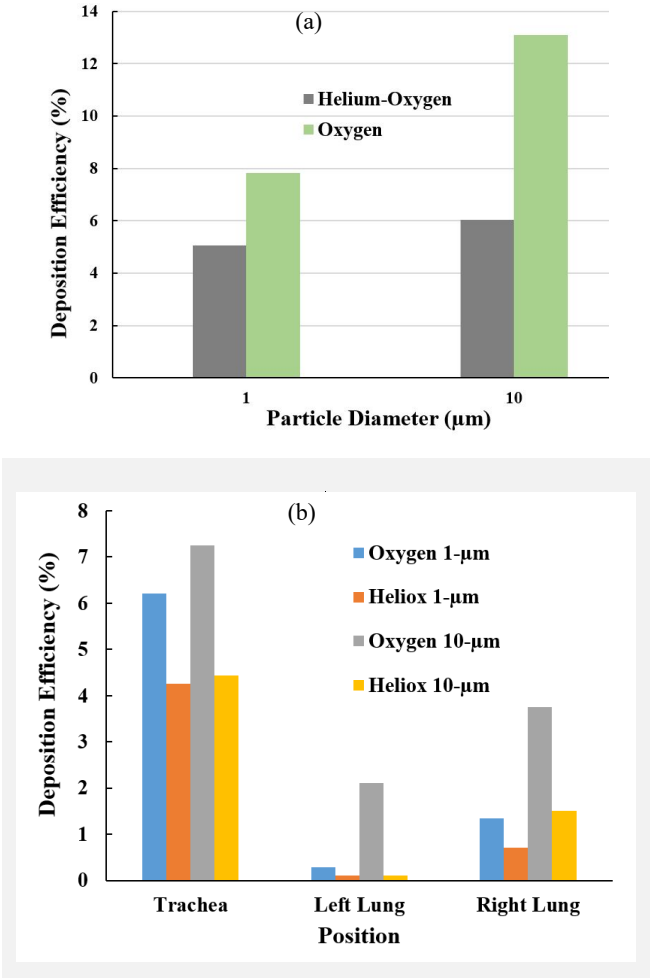

Figure 6: Microparticles DE comparison for air and helium-oxygen breathing; (a) total deposition comparison for 1-µm and 10-µm particles and (b) DE comparison at different position of the lung.

Conclusions

This study performed the numerical investigation of microparticle TD in the upper airways of a realistic anatomical model. Air and helium-oxygen breathing are considered for the present study. The numerical study reports the overall DE at the different region of the upper airway model at 60lpm flow rate. The following conclusions can be drawn from the present study:

- Helium-oxygen breathing shows lower deposition than the air breathing. For 10-µm diameter particle, air-breathing shows the DE is 2.2 times than the helium-oxygen breathing.
- DE at the tracheal wall is higher than the right lung and the left lung. The right lung shows higher deposition compare to the left lung irrespective to the particle size;

The present study will increase the knowledge of particle TD at the upper airways during helium-oxygen breathing. The specific findings will increase the efficiency of the targeted drug delivery as fewer particles are deposited during helium-oxygen breathing.

Acknowledgment

The authors would like to thank the high-performance computing Unit ARC LAB, University of Technology Sydney, Australia.

References

1. Sandeau, J., et al., *CFD simulation of particle deposition in a reconstructed human oral extrathoracic airway for air and helium-oxygen mixtures.* Journal of aerosol science, 2010. **41**(3): p. 281-294.
2. ANDERSON, M., et al., *Deposition in man of particles inhaled in air or helium-oxygen at different flow rates.* Journal of Aerosol Medicine, 1990. **3**(3): p. 209-216.
3. Farhadi Ghalati, P., et al., *Numerical analysis of micro- and nano-particle deposition in a realistic human upper airway.* Comput Biol Med, 2012. **42**(1): p. 39-49.
4. Balásházy, I., W. Hofmann, and T. Heistracher, *Local particle deposition patterns may play a key role in the development of lung cancer.* Journal of Applied Physiology, 2003. **94**(5): p. 1719-1725.
5. Zhang, Z., et al., *Comparison of micro-and nano-size particle depositions in a human upper airway model.* Journal of aerosol science, 2005. **36**(2): p. 211-233.
6. Oldham, M.J., *Computational fluid dynamic predictions and experimental results for particle deposition in an airway model.* Aerosol Science & Technology, 2000. **32**(1): p. 61-71.
7. Martonen, T.B., *Surrogate experimental models for studying particle deposition in the human respiratory tract.* 1985: US Government Printing Office.
8. Greenblatt, E.E., et al., *Regional ventilation and aerosol deposition with helium-oxygen in bronchoconstricted asthmatic lungs.* Journal of aerosol medicine and pulmonary drug delivery, 2016. **29**(3): p. 260-272.
9. Darquenne, C. and G.K. Prisk, *Aerosol deposition in the human respiratory tract breathing air and 80: 20 heliox.* Journal of aerosol medicine, 2004. **17**(3): p. 278-285.
10. Wilcox, D.C., *Turbulence modeling for CFD.* Vol. 2. 1998: DCW industries La Canada, CA.
11. Islam, M.S., et al., *Pulmonary aerosol transport and deposition analysis in upper 17 generations of the human respiratory tract.* Journal of Aerosol Science, 2017. **108**: p. 29-43.